Journal of Environmental Management 354 (2024) 120336

Contents lists available at ScienceDirect

Journal of Environmental Management

journal homepage: www.elsevier.com/locate/jenvman

Research article

Highly efficient heterogeneous electro-Fenton reaction for tetracycline degradation by Fe–Ni LDH@ZIF-67 modified carbon cloth cathode: Mechanism and toxicity assessment

Shuting Cheng [a,b], Bingqing Wu [a], Yuehong Pang [a,*], Xiaofang Shen [a,b,**]

[a] State Key Laboratory of Food Science and Resources, School of Food Science and Technology, Collaborative Innovation Center of Food Safety and Quality Control in Jiangsu Province, Jiangnan University, Wuxi, 214122, China
[b] International Joint Laboratory on Food Safety, Jiangnan University, Wuxi, 214122, China

ARTICLE INFO

Handling Editor: Raf Dewil

Keywords:
Heterogeneous electro-Fenton
Carbon cloth
Hydrogen peroxide
Degradation
Tetracycline

ABSTRACT

In this work, a novel and efficient Fe–Ni LDH@ZIF-67 catalyst modified carbon cloth (CC) cathode was developed for tetracycline (TC) degradation in heterogeneous electro-Fenton (Hetero-EF) process. Compared to Fe–Ni LDH/CC (75.7%), TC degradation rate of Fe–Ni LDH@ZIF-67/CC cathode increased to 95.6% within 60 min. The synergistic effect of hetero-EF and anodic oxidation process accelerated electron transfer, the maximum H_2O_2 production of Fe–Ni LDH@ZIF-67/CC electrode reached 264 mg/L, improving utilization efficiency of H_2O_2. The cathode possessing a satisfied TC degradation performance over a wide pH (3–9). Free radical capture experiment revealed the collaboration of $\cdot O_2^-$, $\cdot OH$, and $^1O_2$ play a significant role in TC degradation. The 5 cycles experiment and metal ion leaching experiment showed that the proposed Fe–Ni LDH@ZIF-67/CC has good recyclability and stability. In addition, the proposed Fe–Ni LDH@ZIF-67/CC cathode achieved satisfying performance in real water (tap water: 97.3%, lake water: 97.7%), demonstrating the possibility for practical application. TC degradation pathways were proposed by theory analysis and experimental results. The toxicity of TC intermediates was reduced by Hetero-EF degradation according to Toxicity Estimation Software Tool and *Escherichia coli* growth inhibition experiments. This work provides a novel modified cathode to improve removal efficiency of antibiotics in wastewater.

1. Introduction

Nowadays, excessive use of antibiotics has led to contamination in water bodies, which posed significant risks to ecosystem and human health (Liu et al., 2018; Pan et al., 2019). Tetracycline (TC), a highly effective broad-spectrum antibiotic, has been widely used in aquaculture, medicine cure and animal husbandry (Ao et al., 2019; Pacheco-Álvarez et al., 2022; Xu et al., 2016). However, TC overuse has led to a series of water pollution, and even caused drug resistance in bacteria, which has threated ecosystem and human health (Harnisz et al., 2015; Zhou et al., 2020). Highly efficient TC removal is challenging for traditional water treatment owing to its stable molecular structure of aromatic ring (Huang et al., 2020). Therefore, improving TC elimination efficiency in wastewater is urgently essential.

Various water treatment methods, such as biological degradation (Shao et al., 2019; Chen et al., 2023), adsorption (Jiang et al., 2023; Canevesi et al., 2020), photocatalysis (Zheng et al., 2022) and electrochemical advanced oxidation processes (EAOPs) (Xin et al., 2022) have been investigated and applied to TC removal. However, biological degradation is time-consuming, the removal of adsorption is incomplete, photocatalysis can cause secondary pollution to a certain degree. Among, EAOPs have attracted more attention in water treatment due to the high efficiency and versatility. Electro-Fenton (EF) had recognized as an environmentally friendly technique of EAOPs (Oturan and Aaron, 2014; Xia et al., 2021; Zhao et al., 2023). The EF process could generate hydrogen peroxide (H_2O_2) in situ by two-electron redox on the cathode (Eq. (1)), which could react with Fe^{2+} to produce hydroxyl radical ($\cdot OH$) to degrade pollutants (Eq. (2)). Fe^{3+} can be reduced at the cathode (Eq.

---

* Corresponding author.
** Corresponding author. State Key Laboratory of Food Science and Resources, School of Food Science and Technology, Collaborative Innovation Center of Food Safety and Quality Control in Jiangsu Province, Jiangnan University, Wuxi, 214122, China.
E-mail addresses: yhpang@jiangnan.edu.cn (Y. Pang), xfshen@jiangnan.edu.cn (X. Shen).

https://doi.org/10.1016/j.jenvman.2024.120336
Received 28 October 2023; Received in revised form 26 January 2024; Accepted 8 February 2024
Available online 16 February 2024
0301-4797/

(3)), which could significantly accelerate Fe^{3+}/Fe^{2+} cycling and ·OH formation (Hu et al., 2021; Luo et al., 2020). However, addition of soluble Fe^{2+}, narrow pH range (2.7–3.2), and the unrecyclable catalyst limit further application of traditional electro-Fenton (Cao et al., 2020; Gao et al., 2015; Sklari et al., 2015). Heterogeneous electro-Fenton (Hetero-EF), due to advantages of less formation of iron sludge, high removal efficiency, has been recognized as a promising water treatment (Hu et al., 2021; Qin et al., 2023b; Zhao et al., 2012). Therefore, exploring effective iron-based heterogeneous catalyst for electrocatalytic generation of H_2O_2 in the EF system has become a key issue.

$$O_2 + 2H^+ + 2e^- \rightarrow H_2O_2 \tag{1}$$

$$H_2O_2 + Fe^{2+} + H^+ \rightarrow Fe^{3+} + \cdot OH + H_2O \tag{2}$$

$$Fe^{3+} + e^- \rightarrow Fe^{2+} \tag{3}$$

In general, Hetero-EF mainly relies on transition metal elements, such as Fe, Co, Mn, loaded on the surface of cathode to catalyze reaction. The transition metal element doping as bimetallic electrodes showed great activity for efficient contaminant removal (Ren et al., 2015; Zhang et al., 2020). Liu et al. prepared Co/Fe co-doped porous graphitic carbon nanocomposites to degrade rhodamine B using micro electrolysis-Fenton method (Liu et al., 2021b). Du et al. synthesized the Fe/Cu-MOFs to degrade sulfamethazine (Du et al., 2021a). Layered double hydroxides (LDHs) are a class of two-dimensional transition metal nanomaterial, raising considerable interest owing to their tunable chemical compositions, high specific surface area, and environmental friendliness (Liu et al., 2020; Poudel and Kim, 2022). Moreover, the modification of LDHs materials with other porous materials can further enhance the surface properties of the composites and significantly improve catalytic performance, such as bimetallic materials. Monometallic iron catalysts modified with multivalent metals such as Cu, Mn, Co, Ni, and Ce present an incremental Hetero-EF activity through more reaction centers (Chen et al., 2019b; Ghasemi et al., 2019; Ishizaki et al., 2020; Xu et al., 2023). In particular, FeNi-based layered bimetallic hydroxides have been of interest as they are considered to be one of the most active electrocatalysts in oxidation-reduction reaction (Li et al., 2019; Peng et al., 2021).

However, LDH has a tendency of self-aggregation and low electrical conductivity, which limit its catalytic activity (Wu et al., 2022). Owing to the large surface area, high porosity and good catalytic activity, zeolitic imidazolate framework-67 (ZIF-67) attract attention in catalysis. In order to solve the defects of LDH materials, Fe–Ni LDH@ZIF-67 composites were synthesized by in-situ growing ZIF-67 on Fe–Ni LDH. Fe–Ni LDH@ZIF-67 catalyst was coated on carbon cloth (CC) by dropping the catalyst ink, it solves the recycling problem of dispersed catalyst and it will not cause secondary pollution. The usage amount of catalyst is also saved a lot compared with the published literature (Ye et al., 2023; Zhang et al., 2022a).

In this study, TC served as a model pollutant, Fe–Ni LDH@ZIF-67/CC cathode was used to improve the activation of H_2O_2 and efficiency of TC degradation in hetero-EF system. The influence of critical factors, degradation performance, the stability and reusability of Fe–Ni LDH@ZIF-67/CC were systematically investigated. The TC removal in real water was also studied. Moreover, the TC degradation mechanism, pathway and ecotoxicity in hetero-EF system were investigated.

2. Experimental section

2.1. Materials and methods

The detailed materials, characterizations, and analytical methods are described in Text S1, S2.

2.2. Synthesis of catalysts and electrode modification

The schematic diagram of the synthesis of Fe–Ni LDH@ZIF-67 is shown in Fig. 1a. The Fe–Ni LDH@ZIF-67 catalyst was fabricated by a facile two-step synthetic route. First, Fe–Ni LDH was prepared via hydrothermal method as Zhu's report with some modification (Zhu et al., 2021). Ni $(NO_3)_2 \cdot 6H_2O$ (10 mM), Fe $(NO_3)_3 \cdot 9H_2O$ (5 mM), and urea (35 mM) were mixed and dissolved in 100 mL deionized water. The mixed solution was then maintained at 100 °C for 24 h. After cooling naturally, it was washed by ethanol and deionized water, dried at 60 °C for 12 h to obtain Fe–Ni LDH. 0.2 g Fe–Ni LDH, 1.314 g of 2-methylimidazole, and 0.582 g of Co $(NO_3)_2 \cdot 6H_2O$ was dissolved in 60 mL of methanol solution. Afterwards, the product was washed and centrifuged, dried at 60 °C for 12 h to obtain Fe–Ni LDH@ZIF-67 for further use.

For the preparation of electrode, CC was washed with acetone, ethanol and deionized water, and dried at 60 °C for 6 h. Then, Fe–Ni LDH@ZIF-67 (20 mg), ethanol (20 μL), and PTFE emulsion (980 μL) were mixed in proportion ultrasound as catalyst ink. The cathode was prepared by dropping the catalyst ink (200 μL) onto bare CC, and the loading amount of catalyst was 1 mg/cm^2. The obtained electrode drying overnight was Fe–Ni LDH@ZIF-67/CC cathode (Fig. 1b). The drying process were all conducted in a vacuum oven.

2.3. Electrochemical measurements

The electrochemical performances of electrodes were measured by cyclic voltammetry (CV) and linear sweep voltammetry (LSV). These measurements were proceeded in aqueous electrolyte (0.05 M Na_2SO_4 solution). CV analysis was performed in N_2 or O_2 saturated Na_2SO_4 solution over a potential scan range of −0.4–1.5 V at a scan rate of 50 mV s^{-1}. LSV measurement was carried with different cathodes at the same scan rate. To further estimate the electrical conductivity of catalyst, bare CC, Fe–Ni LDH/CC and Fe–Ni LDH@ZIF-67/CC were compared in 1 mM $[Fe\ (CN)_6]^{3-/4-}$ solution. All electrochemical measurements were conducted on a traditional three-electrode system, with the working electrode as the electrode to be measured, while equipped with saturated calomel electrode as a reference electrode, and platinum (Pt) sheet as a counter electrode.

2.4. TC degradation experiments

The experiments of TC degradation were carried out in a 150 mL single chamber glass cell. The anode was a Pt sheet (1 cm × 2 cm), and cathode was modified CC (2 cm × 2 cm), the DC power supplied for constant current power through the connection of electrode clamps (Fig. 1b). The initial TC concentration was 10 mg/L, Na_2SO_4 solution (0.05 M) was served as the supporting electrolyte, and stirring rate was set as 600 r/min. The high-pressure gas container was used to continuously provide the needed O_2 (0.4 L/min) of the reaction for in-situ production of H_2O_2, started 10 min before degradation experiment to maintain a steady O_2 concentration. The samples were taken and filtered through the membrane filter (0.22 μm) at defined time intervals for subsequent analysis.

2.5. Density functional theory (DFT) calculation

The detailed DFT calculation can be found in Text S4.

3. Results and discussion

3.1. Analysis of structure and characteristics

The morphology of synthesized Fe–Ni LDH@ZIF-67 was investigated by scanning electron microscopy (SEM) and transmission electron microscopy (TEM). In Fig. 1c and d, it is observed that ZIF-67 crystals are well dispersed and embedded into the surface of Fe–Ni LDH. The Fe–Ni

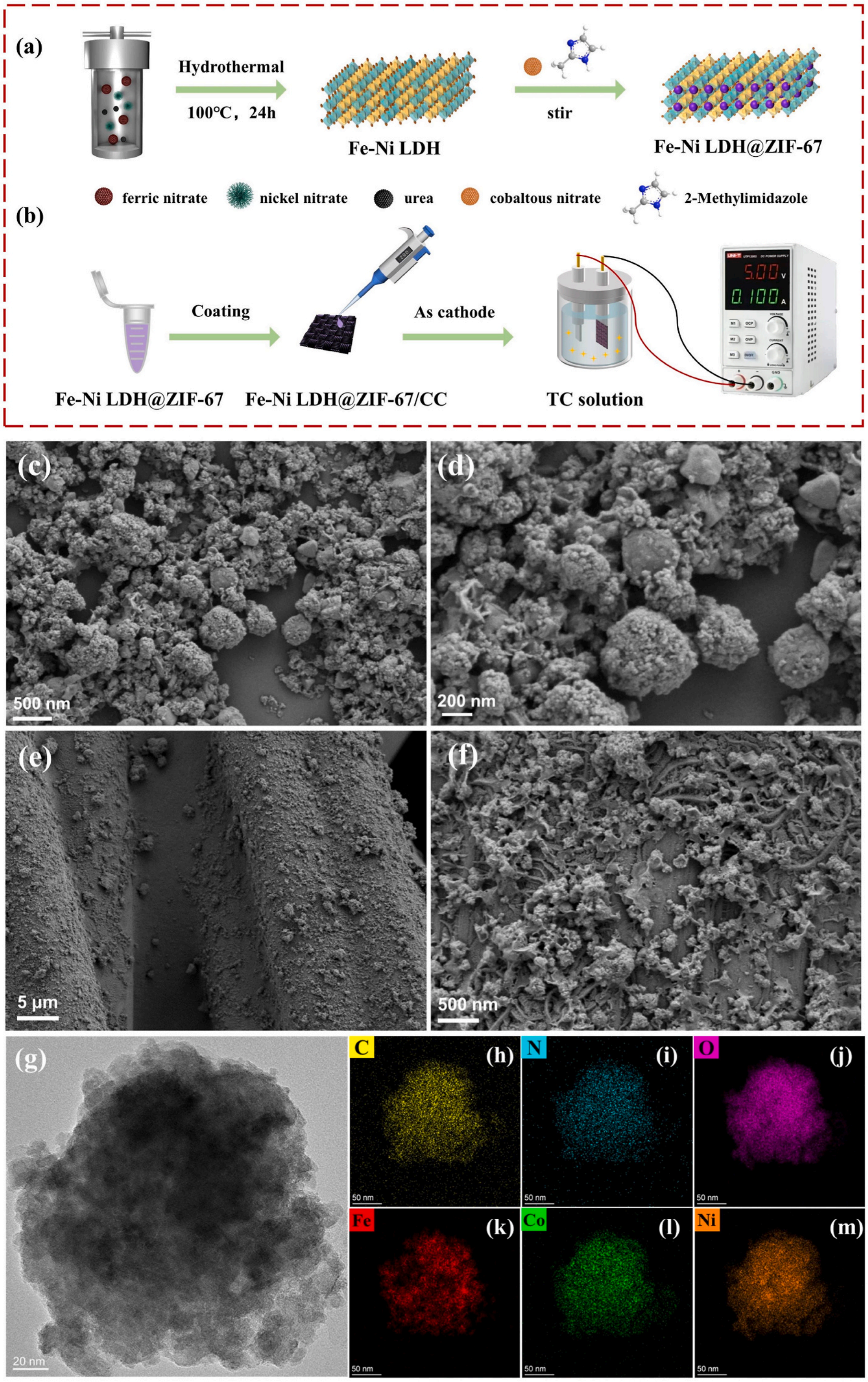

Fig. 1. The scheme of (a) the synthesis of Fe–Ni LDH@ZIF-67catalyst and (b) the preparation process of Fe–Ni LDH@ZIF-67/CC cathode and TC degradation process; SEM images of (c–d) Fe–Ni LDH@ZIF-67; (e–f) Fe–Ni LDH@ZIF-67/CC; (g) TEM image of Fe–Ni LDH@ZIF-67; (h–m) elemental mapping images correspond to C, N, O, Fe, Co and Ni element, respectively.

LDH and partial enlarged SEM image of Fe–Ni LDH@ZIF-67 was provided in Figs. S1 and S2. Fig. S3 shows that the raw CC substrate has a smooth carbon fiber structure. After loading the catalyst on the substrate, the morphology of as-prepared Fe–Ni LDH@ZIF-67/CC are exhibited in Fig. 1e and f. Some nanoparticles were distributed on the surface of CC, and the textural surface became rough, which provided the possibility to accelerate electron transfer in the catalytic process. TEM characterization of Fe–Ni LDH@ZIF-67 (Fig. 1g) showed the darker ZIF-67 crystals could be clearly seen inside the Fe–Ni LDH, indicating its successful composite. Fig. 1h-m showed uniform distribution of C, N, O, Fe, Co and Ni elements of Fe–Ni LDH@ZIF-67, revealing its successful synthesis. Simultaneously, energy dispersive spectroscopy analysis showed that the relative atomic content of elements was 17.90%, 2.87%, 59.41%, 5.70%, 2.80% and 11.32%, respectively (Table S1).

X-ray photoelectron spectroscopic (XPS) spectra explored chemical compositions of Fe–Ni LDH@ZIF-67, and full scan is shown in Fig. 2a. In Fig. 2b, C 1 s spectrum was divided into 4 primary peaks at 284.8, 285.9, 287.5 and 289.4 eV, corresponding to C–C, C–N, C–O and C═O groups

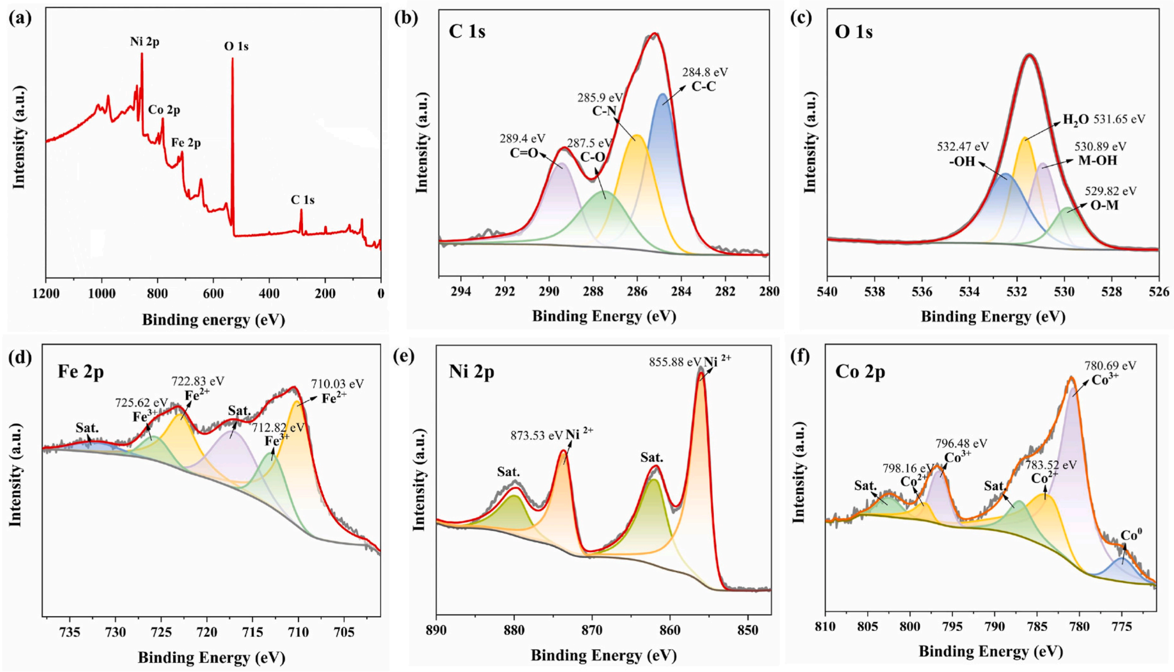

Fig. 2. XPS spectra of Fe–Ni LDH@ZIF-67: (a) full scan; (b) C 1s; (c) O 1 s; (d) Fe 2p; (e) Ni 2p and (f) Co 2p.

respectively (Zhang et al., 2021). Among them, the main peak corresponding to C–C was confirmed by many studies to promote the production of H_2O_2 by 2e$^-$ ORR (Zhao et al., 2023). In Fig. 2c, O 1 s spectrum was classified into four different oxygen species: 529.82 eV, 530.89 eV, 531.65 eV and 532.47 eV, which corresponded to oxygen-metal bonds (O-M), metal-hydroxide bonds (M-OH), adsorbed water and the surface hydroxyl (-OH) (Li et al., 2023; Wang et al., 2022). It indicated that the surface of Fe–Ni LDH@ZIF-67 is conducive to adsorb oxygen to capture electrons and generate more ·OH. For Fe 2p spectra, the major force in EF reaction, Fe^{2+} peaks were at 710.03 and 722.83 eV, Fe^{3+} peaks were at 712.82 and 725.62 eV (Fig. 2d), accompanying by satellite peaks of 716.95 and 731.82eV (Li et al., 2022). Fig. 2e illustrated Ni 2p spectra of catalyst, Ni 2p3/2 and Ni 2p1/2 peaks were located at 855.88 and 873.53 eV, indicating the valence states of Ni^{2+}, which accompanied by two satellite peaks (Yan et al., 2023). The Co 2p spectra of catalyst were fitted with the characteristic peaks at 780.69/796.48 and 798.16/783.52 eV (Fig. 2f), belonging to Co^{3+}/Co^{2+}, respectively (Guo et al., 2022). These metal elements were favorable to generate reactive oxygen species (ROS) and improve the degradation efficiency through EF reaction (Chai et al., 2023). The XPS spectra of bare CC and Fe–Ni LDH@ZIF-67/CC is showed in Fig. S4, further illustrating Fe–Ni LDH@ZIF-67 catalyst was successful loaded on CC.

Fourier transform-infrared (FT-IR) was conducted to characterize functional groups on surfaces of catalyst. In Figs. S5a and a strong characteristic peak at 3435 cm^{-1} was O–H stretching vibration (Gao et al., 2023). For Fe–Ni LDH, the peak at 1576 cm^{-1} was corresponded to C=O vibration of carboxylate groups (Ye et al., 2023). The absorption peak at 749 cm^{-1} represented C–H bending vibration (Mahmoodi et al., 2019). The peak at 690 cm^{-1} was a tensile vibration with N–H bond. The peaks at 1385 cm^{-1} and 831 cm^{-1} were specific absorption bands associated with the nitrate anions, which were produced by the symmetric stretching vibration of the N–O bond in nitrate (Zhong et al., 2023). For Fe–Ni LDH@ZIF-67, the C=O peak stretching vibration result in the significant shift in the position. The absorption peaks at 992, 1137, 1301 and 1416 cm^{-1} ascribed to C–H bending mode and C–N stretching mode of imidazole (Elsonbaty et al., 2021; Su et al., 2020). The peak at 752 cm^{-1} was the stretching vibration of Co–N bond. The presence of above new peaks indicated the successful loading of ZIF-67 nanocrystals on Fe–Ni LDH.

The crystal structure was further investigated by using X-ray diffractometer (XRD). In Fig. S5b, XRD spectrum of Fe–Ni LDH clearly showed three diffraction peaks with the corresponding 2θ values of 11.41, 33.54, and 38.99°, which were associated to (003), (101) and (015) planes of Fe–Ni LDH (JCPDS#40–0215), and it similar with the Fe type LDH materials (Feng et al., 2023; Jia et al., 2023). In addition, the obvious diffraction peaks at 7.366, 10.42, 12.78 and 18.11° corresponded to (011), (002), (112) and (222) planes of ZIF-67 (JCPDS#67–1073) (Gross et al., 2012). Besides, there was no significant peak shift at Fe–Ni LDH@ZIF-67, confirming that the composite of ZIF-67 did not destroy the crystal structure of LDH, which indicated the successful synthesis of catalyst.

The N_2 adsorption-desorption isotherms of catalyst is shown in Fig. S6. On basis of the type IV isotherms, Fe–Ni LDH@ZIF-67 was regarded as mesoporous material. The surface area of catalyst is 57.9 m^2 g^{-1}, with an average pore size of 9.59 nm, there was a certain increase compared to other LDH based catalyst (Xu et al., 2023; Xiong et al., 2023). It was favorable for contacting with active site and solution, thus conducive to the mass transfer between catalyst and electrolyte solution (Zhao et al., 2023). The wettability of CC and Fe–Ni LDH@ZIF-67/CC was investigated in Fig. S7. The contact angles of CC and Fe–Ni LDH@ZIF-67/CC were 142.56° and 104.36°, respectively. It suggested that the hydrophobicity of Fe–Ni LDH@ZIF-67/CC was slightly decreased compared with CC. It could facilitate the rapid penetration of electrolyte into the surface of Fe–Ni LDH@ZIF-67/CC, accelerate O_2 diffusion and promote H_2O_2 formation to accelerate electron transfer in EF process (Zhu et al., 2019; Cui et al., 2020).

3.2. *The electrochemical properties of the electrodes*

CV testing was conducted to estimate electrocatalytic property of the proposed electrodes. In Fig. 3a, Fe–Ni LDH@ZIF-67/CC electrode had an obviously pair of oxidative/reductive peaks compared to bare CC and Fe–Ni LDH/CC electrode, indicating its high electrochemical activity. As for the catalyst loaded electrode, an obvious reduction peak appeared under O_2 saturated condition (Fig. 3b), indicating that the Fe–Ni

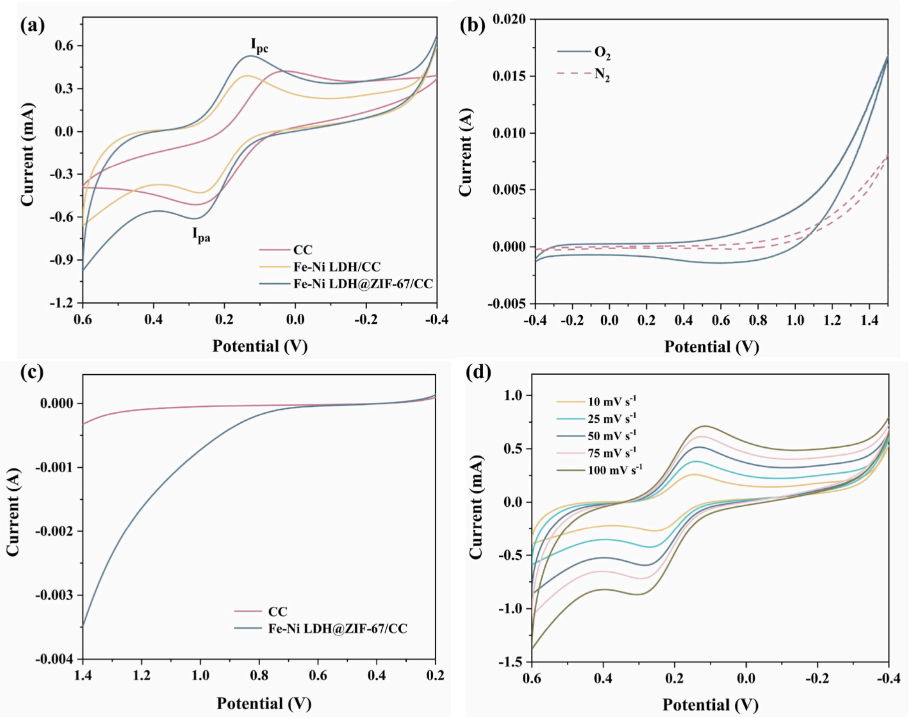

Fig. 3. CV curves of (a) CC, Fe–Ni LDH/CC and Fe–Ni LDH@ZIF-67/CC in 1 mM [Fe $(CN)_6]^{3-/4-}$ solution and (b) Fe–Ni LDH@ZIF-67/CC in O_2/N_2 saturated Na_2SO_4 solution; (c) LSV curves of CC and Fe–Ni LDH@ZIF-67/CC; (d) CV curves of Fe–Ni LDH@ZIF-67/CC at various scan rates.

LDH@ZIF-67/CC electrode possessed good electrochemical activity (Daniel et al., 2020).

As exhibited in Fig. 3c, Fe–Ni LDH@ZIF-67/CC showed a larger current response comparing with bare CC, demonstrating that Fe–Ni LDH@ZIF-67 possessed good electrochemical reaction performance on account of the redox cycle of Fe^{3+}/Fe^{2+}. The redox cycle could provide Fe^{2+} to catalyze H_2O_2, promoting the production of ROSs. In Fig. 3d, CV curves are shown for Fe–Ni LDH@ZIF-67/CC at different scanning rates (10–100 mV s^{-1}) with a potential range (−0.4–0.6 V), conducting in a 1 mM [Fe $(CN)_6]^{3-/4-}$ solution. The linear relationship between peak

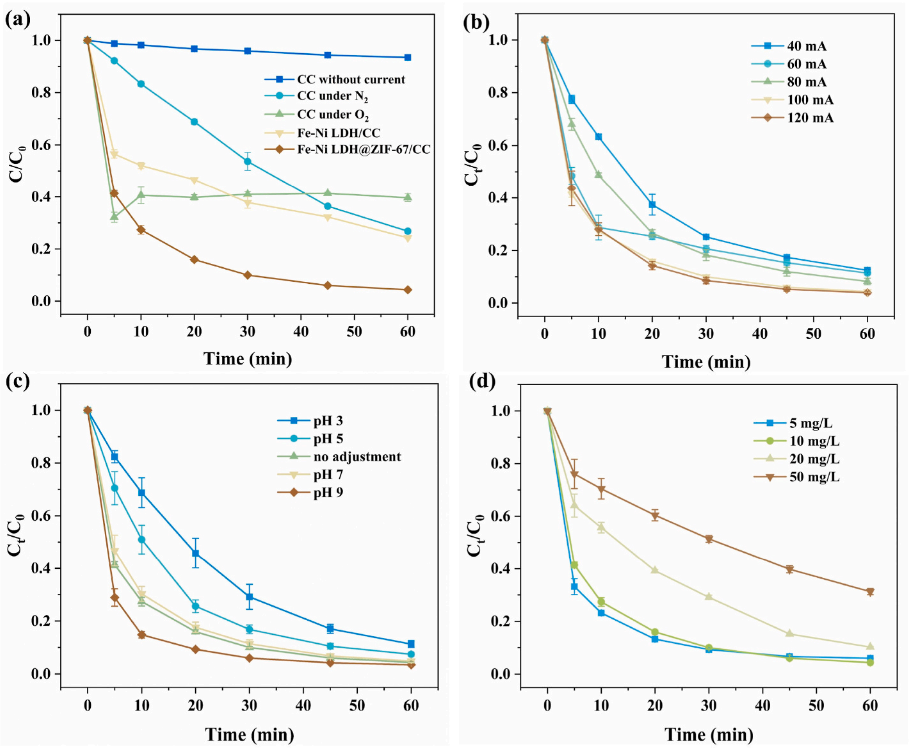

Fig. 4. Effect of (a) different electrodes; (b) applied current; (c) initial pH of solution and (d) initial of TC concentration on TC degradation by hetero-EF process. Reaction parameters: [initial TC concentration] = 10 mg/L, [applied current] = 100 mA, [pH without adjustment] = 6, $[Na_2SO_4]$ = 0.05 M.

current and scan rate$^{1/2}$ ($R^2 = 0.997$) was greater than the scan rate ($R^2 = 0.995$) (Fig. S8), suggesting that the diffusion process was predominant in Fe–Ni LDH@ZIF-67/CC electrode (Li et al., 2021; Wang et al., 2023).

3.3. Catalytic performance of the cathode for hetero-EF reactions

Compared with the degrading efficiency of Fe–Ni LDH/CC (75.7%), Fe–Ni LDH@ZIF-67/CC cathode performed better degradation activity (95.6%) (Fig. 4a), demonstrating the composite of ZIF-67 effectively increased the degradation efficiency. Fe–Ni LDH@ZIF-67/CC cathode can achieve the relatively good degradation efficiency in a short reaction time compared with other reported LDH materials (Table S5).

In EF process, effects of operation conditions, including applied current, pH, and initial concentration of TC were investigated with Fe–Ni LDH@ZIF-67/CC cathode. TC removal gradually increased from 88% to 96% when the current increased from 40 mA to 100 mA (Fig. 4b). It suggested that the incremental current can accelerate electron transfer and redox cycle of catalyst, which is contribute to the production of strong oxidizing free radicals, thus promoting TC degradation. When the current was 120 mA, TC removal remained unchanged with 96.1%, owing to the hydrogen evolution and excessive H_2O_2 scavenging ·OH (Wang et al., 2023; Ye et al., 2023). Therefore, 100 mA was the applied current density value of subsequent experiment from the perspective of energy-saving.

The influence of pH is exhibited in Fig. 4c. TC degradation efficiency was 88.7%, 92.6%, 95.1%, 96.5% and 95.6% at pH 3, 5, 7, 9 and initial pH without adjustment (pH 6) respectively, indicating that catalyst had satisfied degradation performance over a wide pH range. Compared with homogeneous EF process, Fe–Ni LDH@ZIF-67/CC cathode still showed satisfactory degradation effect under neutral and alkaline conditions, remarkably expanding pH range in hetero-EF systems. The degradation efficiency was better under alkaline condition, which could be explained by the results in Section 3.4, due to $\cdot O_2^-$ played a major role. The pH increase was favorable to the formation of $\cdot O_2^-$, thereby improving TC degradation efficiency (Zou et al., 2023). To avoid operating costs and secondary pollution causing by pH adjustment, the following degradation experiments were conducted without pH adjustment.

The degradation performance gradually improved as the initial TC concentration decreased (Fig. 4d). TC was almost completely removed at low concentration within 60 min, and the degradation rate decreased to 68.8% when TC concentration increased to 50 mg/L. This showed that generated radicals are insufficient for excessive pollutant removal. In addition, the increase of TC concentration led to the covering of active sites on Fe–Ni LDH@ZIF-67, which prevented production of reactive species for TC degradation. Moreover, large numbers of pollutants indicated higher production of intermediates that lead to competitive ·OH consumption, TC removal efficiency will be reduced.

Simultaneously, H_2O_2 production and activation are significant factors in the EF reaction. The yield of H_2O_2 on bare CC and Fe–Ni LDH@ZIF-67/CC was measured under different currents. As shown in Fig. S9, H_2O_2 could be accumulated up to 264 mg/L within 60 min at 100 mA. While at the same conditions, H_2O_2 production of Fe–Ni LDH@ZIF-67 was only 3 mg/L, which demonstrated the activation of H_2O_2 generated speed up transfer of metal ions and trigger the production of ROS and other strong oxidants for TC degradation.

3.4. The hetero-EF mechanism of the Fe–Ni LDH@ZIF-67/CC electrode

The TC removal on bare carbon cloth by adsorption without current, bubbling O_2 and anodic oxidation (bubbling N_2) was tested for reference (Fig. 4a). The removal efficiency was only 6.5% for adsorption without current, 60.4% for effect of oxygen, 73.2% for anodic oxidation, and TC could be degraded by 95.6% in 60 min by electro-Fenton. It indicated that synergistic effect of hetero-EF and anodic oxidation process has a significant contribution to the TC degradation. Various inorganic anions and organic matter are existed in the actual water, which could influence degradation efficiency. The effects of co-existing constituents were investigated in Fig. 5a. The results showed that Cl^- (10 mM) promoted TC degradation in hetero-EF treatment over 60 min, due to the generation of HClO and ClO^- during anodic oxidation process (Eqs. (4)–(6)) (Long et al., 2023). The degradation efficiency declined from 95.6% to 71.6% in the existence of HPO_4^{2-}, mostly owing to slow reaction rate between HPO_4^{2-} and ·OH (Eq. (7)), and generated $HPO_4^{\cdot -}$ cannot effectively oxidize TC (Zhang et al., 2022a). Moreover, the introduction of 10 mM NO_3^- and 10 mg/L humic acid (HA) also inhibited TC degradation to some extent since the production of $NO_3^{\cdot}$ with lower redox potential, and HA competed with pollutants for ·OH (Eq. (8)) (Zhang et al., 2022b).

$$2Cl^- + 2e^- \rightarrow Cl_2 \tag{4}$$

$$Cl_2 + H_2O \rightarrow HClO + H^+ + Cl^- \tag{5}$$

$$Cl_2 + 2OH^- \rightarrow ClO^- + H_2O + Cl^- \tag{6}$$

$$\cdot OH + HPO_4^{2-} \rightarrow HPO_4^{\cdot -} + OH^- \tag{7}$$

$$\cdot OH + NO_3^- \rightarrow NO_3^{\cdot} + OH^- \tag{8}$$

In Fig. 5b, TOC removal efficiency of TC gradually increased with the duration of reaction time, it reached 76.5% within 6 h, indicating that TC is decomposed into a certain number of small organic molecules during hetero-EF process. As exhibited in Fig. 5c, n-butanol, pbenzoquinone (p-BQ), and furfuryl alcohol (FFA) were presented as radical scavengers to remove ·OH, $\cdot O_2^-$, and $^1O_2$ in quenching experiments. Without adding any scavenger, the hetero-EF system can almost completely remove TC after running for 60 min. TC removal rate decreased by only 14% with the introduction of 500 mM n-butanol, which confirmed that ·OH might have a weak effect on TC degradation. When 200 mM FFA was added in reaction, TC degradation rate was reduced to 68.4%. After adding 50 mM p-BQ, degradation rate was reduced to only 48.5%. These results demonstrated that $\cdot O_2^-$, ·OH, and $^1O_2$ exist in TC degradation, and $\cdot O_2^-$ is the dominant active radical (Liu et al., 2021c; Yan et al., 2018).

To further verify production of the above three active species, the spin-trapping agents 5,5-dimethyl-1-pyrrolidine-N-oxide (DMPO) and 2,2,6,6-tetramethylpiperidine (TEMP) were used to record EPR signals. From Fig. 5d–f, the EPR signals of DMPO-·OH, DMPO-$\cdot O_2^-$ and TEMP-$^1O_2$ can be observed clearly. Fig. 5d exhibited the characteristic peak of DMPO-·OH with an intensity ratio of 1:2:2:1 at 5 min. Fig. 5e showed the signal with an intensity ratio of 1:1:1:1, which was in agreement with DMPO-$\cdot O_2^-$ peak. Fig. 5f observed the presence of triplet signals with an intensity ratio of 1:1:1, attributing to TEMP-$^1O_2$ peak. The peak strengths increased with EF reaction, demonstrating H_2O_2 activation has led to the production of ROSs. These were consistent with the results of quenching experiments.

Based on the above results, a possible TC degradation mechanism is exhibited in Fig. 6. Firstly, ·OH could be in situ generated at the surface of anode, which attacked TC around (Qin et al., 2023a). Secondly, O_2 molecules were adsorbed onto Fe–Ni LDH@ZIF-67/CC cathode to generate H_2O_2 in situ through two-electron reduction reaction to form ·OH and Fe^{3+} (Tian et al., 2020). Fe^{3+} got an electron on Fe–Ni LDH@ZIF-67/CC cathode to regenerate Fe^{2+}, which contributed the cycle of Fe^{3+}/Fe^{2+}. Moreover, Ni^{3+}/Co^{3+} also reduced by H_2O_2 to produce ·OH, which formed the Ni^{3+}/Ni^{2+} and Co^{3+}/Co^{2+} cycle at the cathode and enhance utilization efficiency of H_2O_2. Meanwhile, O_2 gained an electron to form $\cdot O_2^-$, which could react with ·OH and H_2O and to form $^1O_2$. Finally, these species mineralized TC into small molecules ((Eqs. 9–13) (Chen et al., 2019a; Wang et al., 2023).

$$Fe^{2+}/Ni^{2+}/Co^{2+} + H_2O_2 \rightarrow \cdot OH + Fe^{3+}/Ni^{3+}/Co^{3+} + OH^- \tag{9}$$

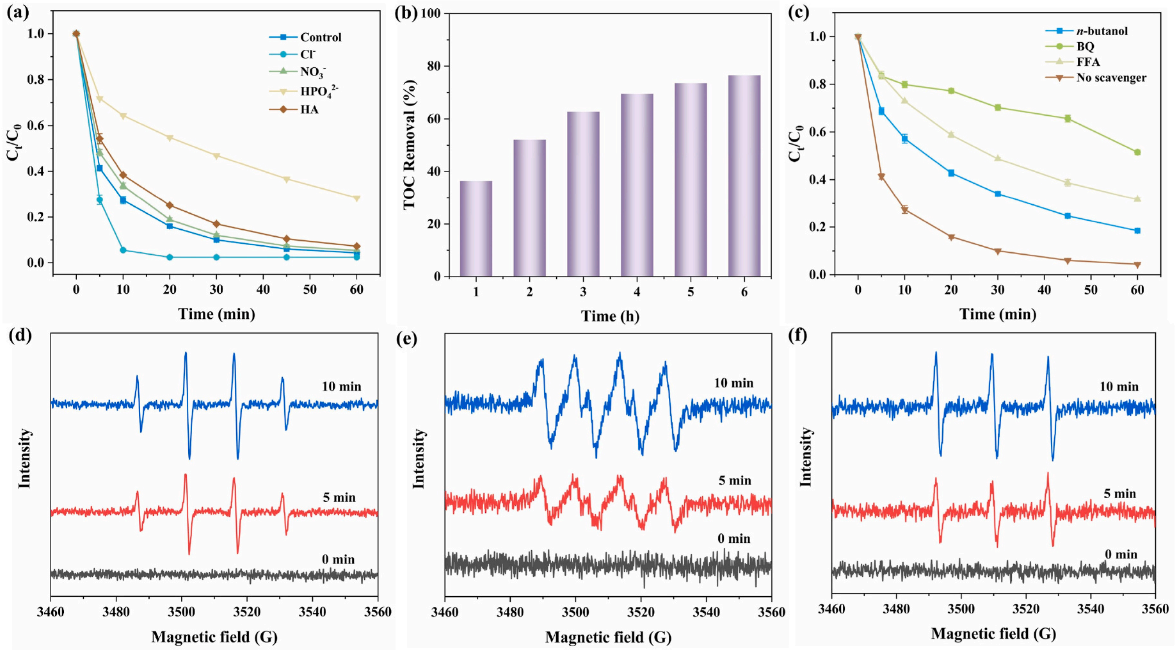

Fig. 5. (a) Effects of co-existing constituents on TC degradation; (b) The TOC removal efficiency of TC; (c) The experiment of radical scavengers; EPR spectra of (d) DMPO-·OH; (e) DMPO-·O_2^- and (f) TEMP-$^1O_2$.

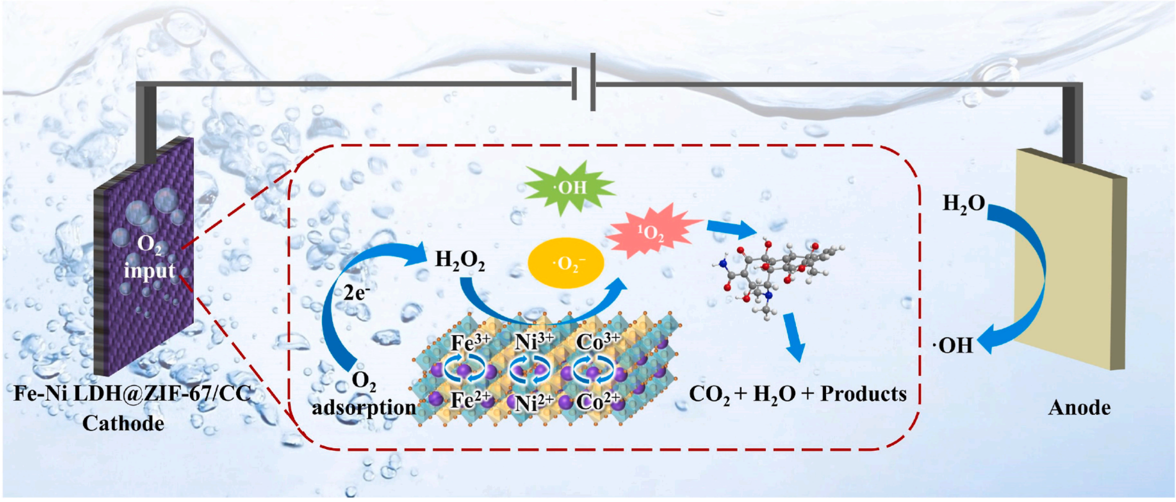

Fig. 6. Proposed mechanism for TC degradation with Fe–Ni LDH@ZIF-67/CC cathode.

$$Fe^{3+}/Ni^{3+}/Co^{3+} + H_2O_2 \rightarrow Fe^{2+}/Ni^{2+}/Co^{2+} + \cdot O_2^- + 2H^+ \quad (10)$$

$$\cdot O_2^- + \cdot OH \rightarrow {}^1O_2 + OH^- \quad (11)$$

$$2 \cdot O_2^- + 2H_2O \rightarrow H_2O_2 + 2OH^- + {}^1O_2 \quad (12)$$

$$\cdot OH \Big/ \cdot O_2^- / {}^1O_2 + TC \rightarrow CO_2 + H_2O + \text{Other products} \quad (13)$$

3.5. The reusability and applicability of Fe–Ni LDH@ZIF-67/CC cathode

Apart from the degradation efficiency, the stability of electrode was also significant in the perspective of practical application. Hence, the reusability of Fe–Ni LDH@ZIF-67/CC was evaluated by continuous five times degradation. As exhibited in Fig. 7a, TC degradation rate remained probably 80% and had not weakened significantly for 5 cycles. During long-term operation, adsorption of some intermediates and loss of active sites result in electrode deactivation. This manifested that the Fe–Ni LDH@ZIF-67/CC cathode was stable and reusable. Moreover, leaching of metal ions from Fe–Ni LDH@ZIF-67/CC electrode is shown in Fig. 7b. Fe, Ni and Co leached from the cathode increased with reaction time, where the maximum value was 0.361, 0.106 and 0.113 mg/L respectively, lower than the limits of European Union standard and water environment discharge standards of China (GB 25467–2010).

In addition, stability of the cathodes was examined by the spectrum of XRD, FT-IR and XPS of the fresh and used cathode before and after cycle experiment. As exhibited in Fig. 7c, there was no obvious change about crystal structure before and after use. Besides, in Fig. 7d, there was no additional characteristic peaks observed and surface molecular structure did not change after degradation. As shown in Fig. S10, it just slightly weak of XPS full scan intensity for the electrode after degradation. These results demonstrated that the Fe–Ni LDH@ZIF-67/CC cathode had good stability.

Furthermore, the performance of cathode was investigated in Fig. 7e

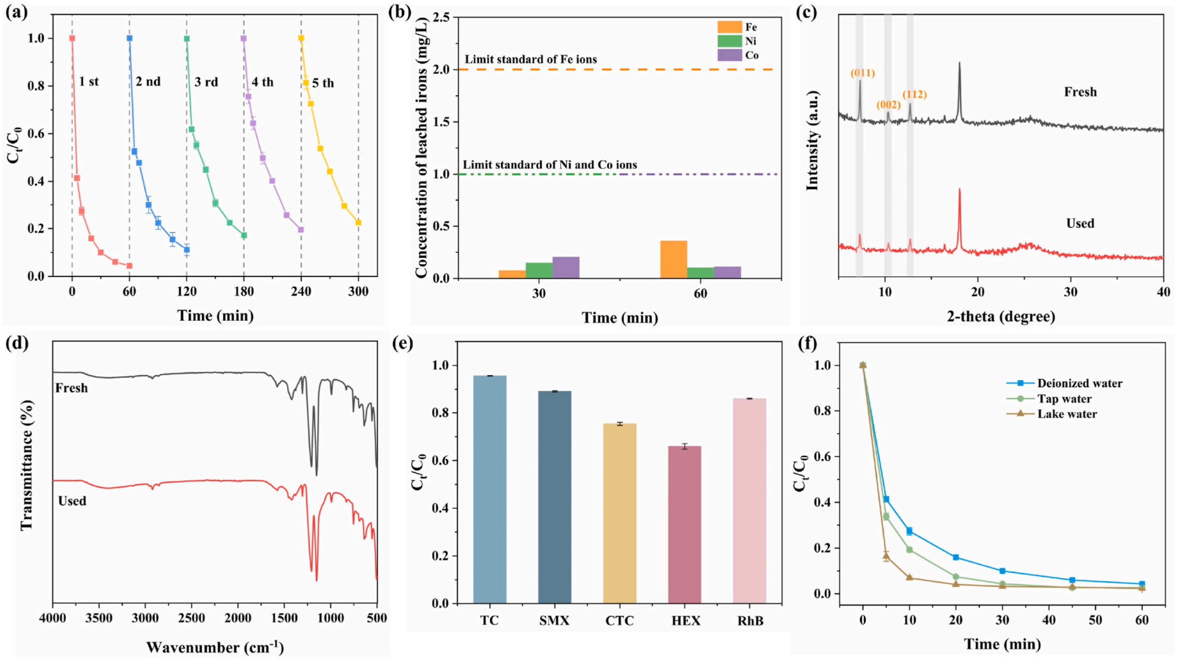

Fig. 7. (a) The stability of the Fe–Ni LDH@ZIF-67/CC cathode; (b) The meatal leaching in hetero-EF process; (c) The XRD patterns and (d) FTIR spectra of Fe–Ni LDH@ZIF-67/CC cathode before and after degradation; (e) The catalytic performance towards on various pollutants in hetero-EF process; (f) TC removal in different actual water.

by degrading other refractory pollutants, including sulfamethoxazole (SMX), chlortetracycline (CTC), hexaconazole (HEX) and rhodamine B (RhB). The removal rates of these pollutants were 89.1, 75.4, 66.0 and 86.1% within 60 min, respectively. The results indicated that Fe–Ni LDH@ZIF-67/CC had broad applicability to degrade multiple pollutants. It is worth mentioning that the hetero-EF system did not optimize the degradation conditions for these four pollutants. Therefore, it can achieve better degradation performance if optimizing of the conditions.

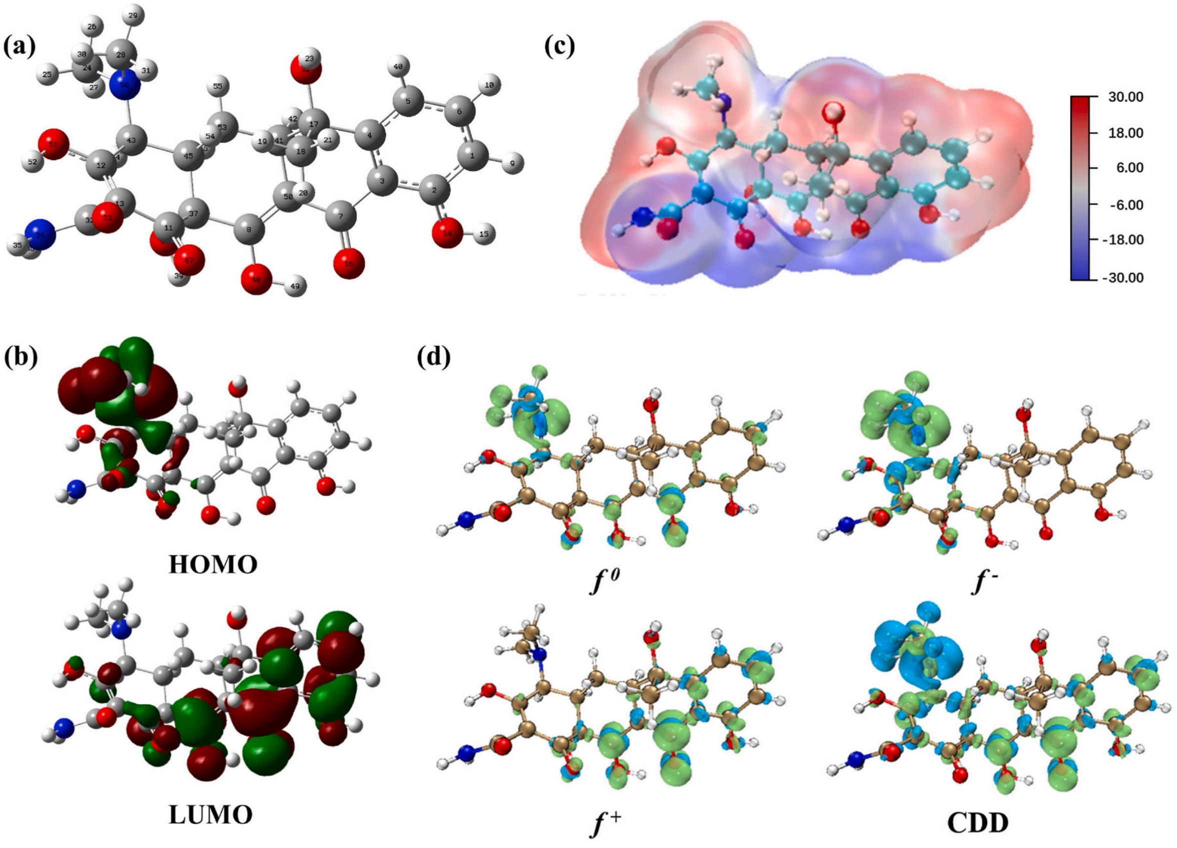

Fig. 8. (a) TC chemical structure; (b) HOMO and LUMO orbital of TC; (c) ESP mapping of TC; (d) The Fukui index (f^0, f^-, f^+ and CDD) of TC.

In order to estimate the potential for treating actual water, TC degradation was investigated using tap water and lake water, and the degradation rates were 97.3% and 97.7% (Fig. 7f), suggesting that Fe–Ni LDH@ZIF-67/CC was able to exhibit excellent performance in actual water. The effect of TC removal in actual water was higher than ultra-pure water, which may be the Cl^- present in the actual sample. Cl^- was oxidized on surface of anode directly to generate active chlorine (Cl_2, ClO^-, Cl·, and HClO) (Eqs. (4)–(6)) (Qi et al., 2022), which participated in the degradation of TC. Therefore, the Fe–Ni LDH@ZIF-67/CC cathode had excellent degradation efficiency in actual water. Furthermore, the proposed hetero-EF method well performed for TC degradation compared with previous works is shown in Table S6. These above results suggested that the proposed hetero-EF method is effective and promising for TC degradation.

3.6. *Degradation intermediates and toxicity assessment*

In order to further elucidate the attack of free radicals on TC molecules, DFT was conducive to accurately identify the degradation pathway. The optimized TC chemical structure is exhibited in Fig. 8a, the corresponding HOMO and LUMO orbitals were shown in Fig. 8b. The green and red region denoted as electron-poor and electron-rich region, respectively. Electrostatic potential (ESP) spectra of TC were shown in Fig. 8c, positive areas (blue regions) and negative (red regions) were considered as the promising reactive sites for oxidation and reduction reactions. The Hirshfeld charges and Fukui index (f^0, f^-, $f^+$and CDD) were calculated in Table S7 and their structures were displayed in Fig. 8d. The higher the values of f^0, f^- and f^+, it is more susceptible to attack the compound by free radicals, electrophiles (·OH, $^1O_2$), and nucleophiles ($\cdot O_2^-$). It can be seen the reactive sites of N56 (f^-= 0.2638), H25 (f^-= 0.0724), H30 (f^-= 0.0679), C24 (f^-= 0.0584) and C28 (f^-= 0.0526) with higher Fukui index, indicating that they were the most active sites and were more susceptible to attacks from electrophilic species. Meanwhile, the reactive sites of O16, O48 C6, C7, and C8 with higher Fukui index were susceptible to nucleophilic reactions.

Subsequently, possible TC degradation pathway was also presented by LC-MS which was used to analyze possible intermediates based on samples were taken at 0, 10, 30, and 60 min (Fig. 9). In pathway I, TC was transformed into P1 (m/z = 417) by demethylation reaction, which then was transformed into P2 (m/z = 401) via the oxidation of ROSs. P3 (m/z = 339) was generated through demethylation and deamination reaction. For pathway II, P4 (m/z = 461) was formed by adding a hydroxyl group. The generation of compounds of P5 (m/z = 477) was generated via hydroxylation reaction (Zhang et al., 2022a). Then, P6 (m/z = 351) was formed by through a series of ROSs attacking and demethylation reaction. For pathway III, P7 (m/z = 509) was acquired

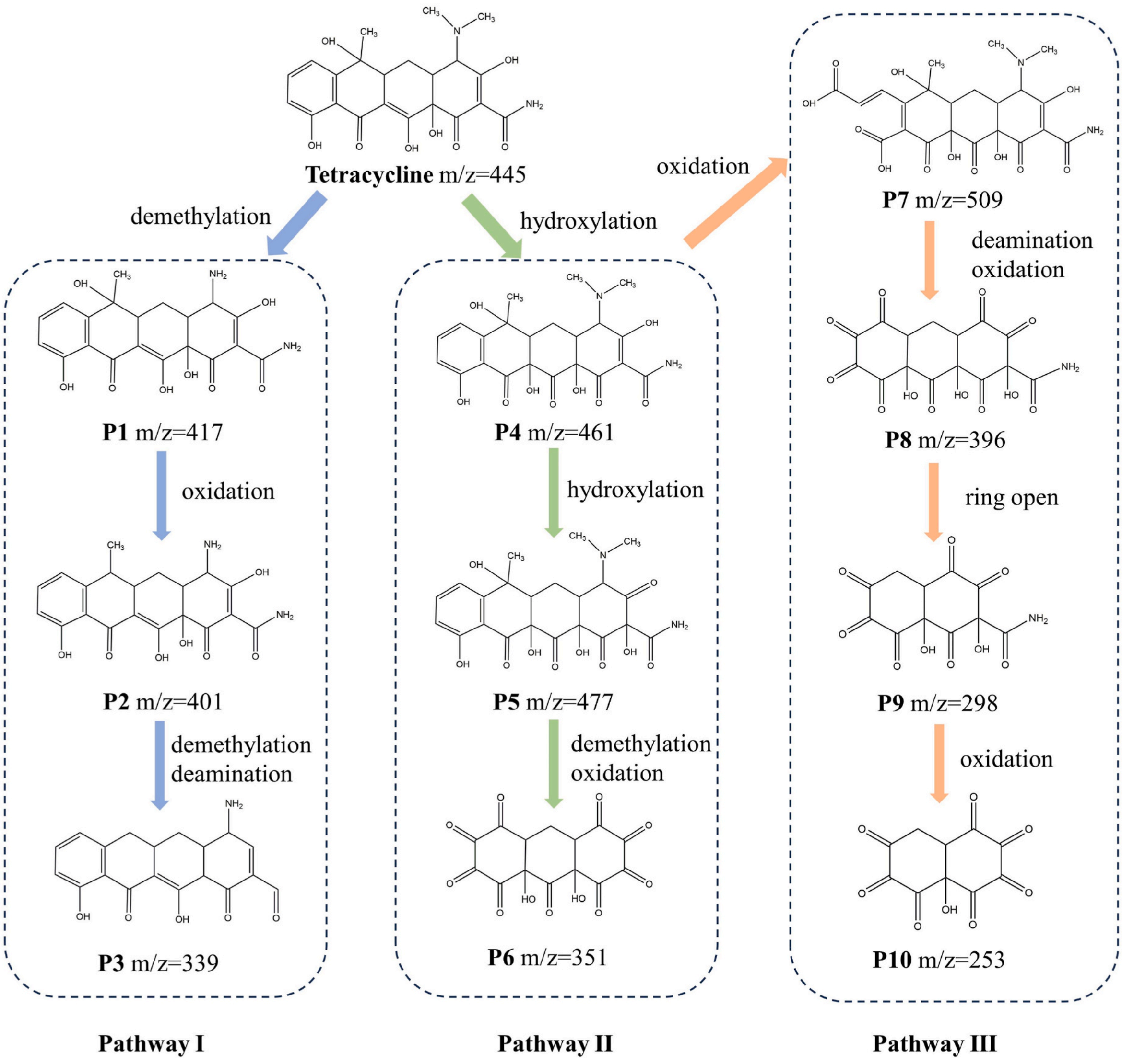

Fig. 9. The proposed TC degradation pathway.

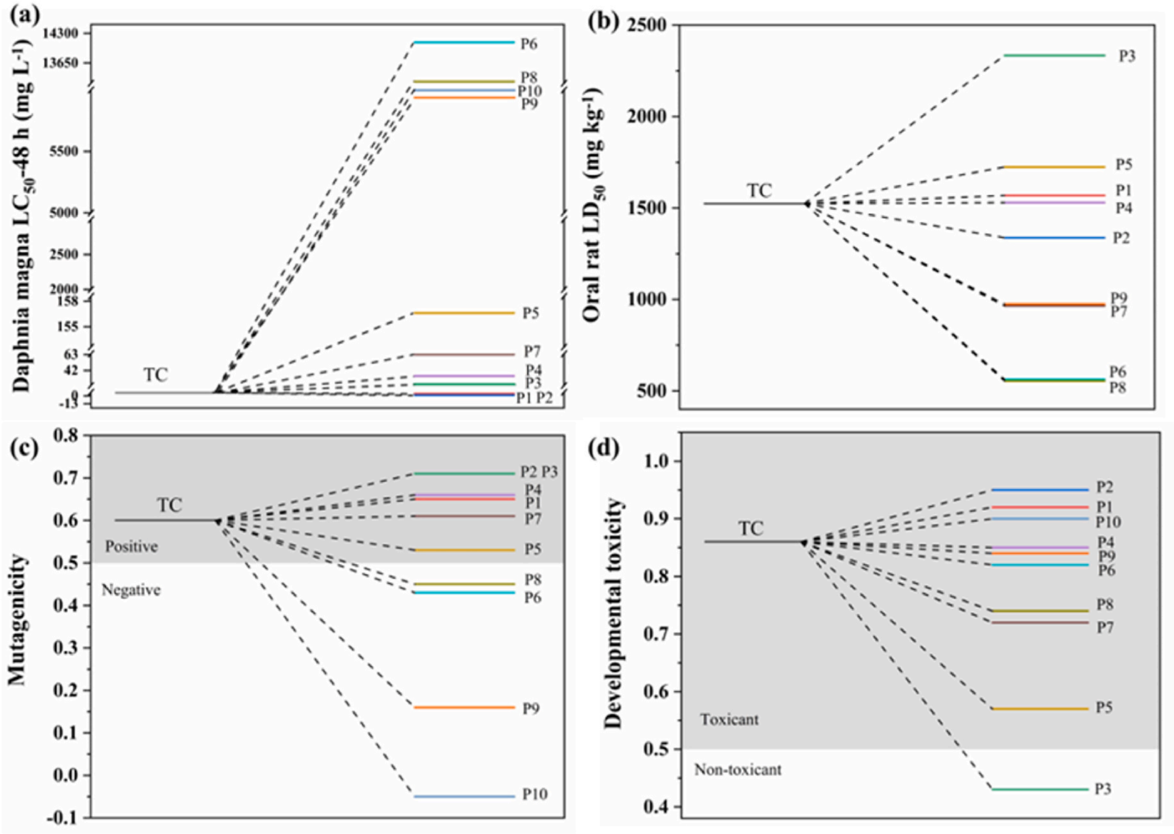

Fig. 10. (a) Daphnia magna LC_{50}-48 h; (b) Oral rat LD_{50}; (c) mutagenicity; (d) developmental toxicity of TC and its intermediates.

by the double bond oxidation of P4 ($m/z = 461$), which generated a ketone group and a carboxyl group (Liu et al., 2021a). Subsequently, P8 ($m/z = 396$) was obtained through deamination oxidization, P9 ($m/z = 298$) was acquired through the ring opening processes (Dai et al., 2022; Du et al., 2021b). P10 ($m/z = 253$) might be produced from intermediate P9 ($m/z = 298$) via the oxidation of ROSs. The mass spectra and information of TC degradation intermediates are shown in Fig. S11 and Table S8. Finally, TC intermediates were eventually mineralized to produce CO_2 and H_2O (Luo et al., 2020; Zhou et al., 2023).

The acute toxicity, mutagenicity and developmental toxicity of TC and its intermediates was estimated by T.E.S.T. software. The values of toxicity assessment of TC and its intermediates by T.E.S.T. are shown in Table S9. As shown in Fig. 10a, Daphnia magna LC_{50} value of TC was 5.4 mg/L, and values of most intermediates increased, indicating the acute toxicity was significantly reduced after TC degradation. In Fig. 10b, oral rat LD_{50} of TC was 1524 mg kg^{-1}, which was tagged as "hypotoxicity". Among the degradation intermediates, P1, P3, P4 and P5 showed reduced acute toxicity compared to TC. Among degradation intermediates, P10 was missing in these estimated results owing to it is N/A for oral rat. Although the acute toxicity of intermediates were elevated and reduced compared to TC, they were overall classified into low toxic category (500–5000 mg kg^{-1}). For the mutagenicity (Fig. 10c), mutagenicity values of P1, P7, P8 and P10 were lower than TC, especially, mutagenicity (<0.5) of P6, P8, P9 and P10 transformed into "negative", which manifested that mutagenicity toxicity was significantly reduced. As exhibited in Fig. 10d, developmental toxicity of most intermediates was significantly lower than TC, except for the intermediates P1, P2 and P10.

The *Escherichia coli (E. coli)* growth inhibition experiments were performed to further investigate toxicity of initial TC solution and solution after degradation through the diameter of inhibition zone (Text S5). The diameter of original TC solution was about 19.0 mm (Fig. S12a). The growth of *E. coli* was obviously inhibited as degradation time increased. Obviously, the inhibition zone was almost disappeared after 60 min degradation (Fig. S12b). The results demonstrated that the content of TC had no effect on bacteria after degradation in hetero-EF system. Therefore, the proposed degradation method is a promising technology for relieving hazards of TC in environment.

4. Conclusion

In this paper, Fe–Ni LDH@ZIF-67 catalyst was modified on CC as cathode for TC removal in hetero-EF system. The catalyst loading increased the active site on the CC, facilitating electron transport and H_2O_2 decomposition. Fe–Ni LDH@ZIF-67/CC cathode had excellent degradation performance over a wide pH range (3–9). $\cdot O_2^-$, $\cdot OH$, and $^1O_2$ were primary ROSs in hetero-EF system, and $\cdot O_2^-$ played a predominant role. The high degradation efficiency and good stability of the hetero-EF system demonstrated its potential for practical applications. DFT calculations and LC-MS measurement proposed the TC degradation pathway. Furthermore, the results of T.E.S.T. prediction and *E. coli* growth inhibition experiments verified the intermediates had lower ecotoxicity, demonstrating the proposed EF degradation method was environmentally safe. This work provided a highly effective and eco-friendly water treatment, making it potential to remove refractory pollutants, and the proposed Fe–Ni LDH@ZIF-67/CC cathode was expected to be a promising EF process for practical applications in large-batch treatment of wastewater.

CRediT authorship contribution statement

Shuting Cheng: Writing – original draft, Methodology, Investigation, Formal analysis, Conceptualization. **Bingqing Wu:** Methodology, Investigation, Formal analysis. **Yuehong Pang:** Writing – review & editing, Methodology, Funding acquisition. **Xiaofang Shen:** Writing – review & editing, Supervision, Project administration.

Declaration of competing interest

The authors declare that they have no known competing financial interests personal relationships that could have appeared to influence the work reported in this paper.

Data availability

Data will be made available on request.

Acknowledgements

This work was supported by the National Natural Science Foundation of China (22276077, 21976070), and the Postgraduate Research & Practice Innovation Program of Jiangsu Province (KYCX23_2515).

Appendix A. Supplementary data

Supplementary data to this article can be found online at https://doi.org/10.1016/j.jenvman.2024.120336.

References

Ao, X., Sun, W., Li, S., Yang, C., Li, C., Lu, Z., 2019. Degradation of tetracycline by medium pressure UV-activated peroxymonosulfate process: influencing factors, degradation pathways, and toxicity evaluation. Chem. Eng. J. 361, 1053–1062. https://doi.org/10.1016/j.cej.2018.12.133.

Canevesi, R., Sanchez, A., Gadonneix, P., Celzard, A., Fierro, V., 2020. Hierarchical tannin-derived carbons as efficient tetracycline adsorbents. Appl. Surf. Sci. 533, 147428 https://doi.org/10.1016/j.apsusc.2020.147428.

Cao, P., Quan, X., Zhao, K., Chen, S., Yu, H., Su, Y., 2020. High-efficiency electrocatalysis of molecular oxygen toward hydroxyl radicals enabled by an atomically dispersed iron catalyst. Environ. Sci. Technol. 54 (19), 12662–12672. https://doi.org/10.1021/acs.est.0c03614.

Chai, Y., Bai, M., Chen, A., Xu, X., Tong, Z., Yuan, J., Peng, L., Shao, J., Xiong, J., Peng, C., 2023. Upcycling contaminated biomass into metal-supported heterogeneous catalyst for electro-Fenton degradation of thiamethoxam: preparation, mechanisms, and implications. Chem. Eng. J. 453, 139814 https://doi.org/10.1016/j.cej.2022.139814.

Chen, C., Ma, T., Shang, Y., Gao, B., Jin, B., Dan, H., Lia, Q., Yue, Q., Li, Y., Wang, Y., Xu, X., 2019a. In-situ pyrolysis of *Enteromorpha* as carbocatalyst for catalytic removal of organic contaminants: considering the intrinsic N/Fe in *Enteromorpha* and non-radical reaction. Appl. Catal. B Environ. 250, 382–395. https://doi.org/10.1016/j.apcatb.2019.03.048.

Chen, G., Nengzi, L. chao, Li, B., Gao, Y., Zhu, G., Cheng, X., 2019b. Octadecylamine degradation through catalytic activation of peroxymonosulfate by Fe-Mn layered double hydroxide. Sci. Total Environ. 695, 133963 https://doi.org/10.1016/j.scitotenv.2019.133963.

Chen, X., Zhu, Y., Chen, J., Yan, S., Xie, S., 2023. Multi-omic profiling of a novel activated sludge strain *Sphingobacterium* sp. WM1 reveals the mechanism of tetracycline biodegradation and its merits of potential application. Water Res. 243, 120397 https://doi.org/10.1016/j.watres.2023.120397.

Cui, L., Huang, H., Ding, P., Zhu, S., Jing, W., Gu, X., 2020. Cogeneration of H_2O_2 and radical ·OH via a novel Fe_3O_4/MWCNTs composite cathode in a dual-compartment electro-Fenton membrane reactor. Sep. Purif. Technol. 237, 116380 https://doi.org/10.1016/j.seppur.2019.116380.

Dai, Y., Yao, Y., Li, M., Fang, X., Shen, C., Li, F., Liu, Y., 2022. Carbon nanotube filter functionalized with MIL-101(Fe) for enhanced flow-through electro-Fenton. Environ. Res. 204, 112117 https://doi.org/10.1016/j.envres.2021.112117.

Daniel, G., Zhang, Y., Lanzalaco, S., Brombin, F., Kosmala, T., Granozzi, G., Wang, A., Brillas, E., Sirés, I., Durante, C., 2020. Chitosan-derived nitrogen-doped carbon electrocatalyst for a sustainable upgrade of oxygen reduction to hydrogen peroxide in UV-assisted electro-Fenton water treatment. ACS Sustainable Chem. Eng. 8, 14425–14440. https://doi.org/10.1021/acssuschemeng.0c04294.

Du, X., Fu, W., Su, P., Su, L., Zhang, Q., Cai, J., Zhou, M., 2021a. Trace FeCu@PC derived from MOFs for ultraefficient heterogeneous electro-Fenton process: enhanced electron transfer and bimetallic synergy. ACS EST Engg 1 (9), 1311–1322. https://doi.org/10.1021/acsestengg.1c00131.

Du, Z., Feng, L., Guo, Z., Yan, T., Hu, Q., Lin, J., Huang, Y., Tang, C., Fang, Y., 2021b. Ultrathin h-BN/Bi_2MoO_6 heterojunction with synergetic effect for visible-light photocatalytic tetracycline degradation. J. Colloid Interface Sci. 589, 545–555. https://doi.org/10.1016/j.jcis.2021.01.027.

Elsonbaty, A., Elshaer, A.M., Harb, M., Soliman, M., Ebrahim, S., Eltahan, A., 2021. Novel ZIF67/Mn/MWCNTs decorated with layer double hydroxide supercapacitor electrodes. Electrochim. Acta 368, 137577. https://doi.org/10.1016/j.electacta.2020.137577.

Feng, Y., Wei, Y., Liu, S., Li, P., Akhtar, K., Bakhsh, E.M., Khan, S.B., Shen, Y., 2023. Enhanced hydrogen evolution reaction activity of FeNi layered double hydroxide modified with Ruthenium nanoparticles at high current density. J. Electroanal. Chem. 938, 117451 https://doi.org/10.1016/j.jelechem.2023.117451.

Gao, G., Zhang, Q., Hao, Z., Vecitis, C.D., 2015. Carbon nanotube membrane stack for flow-through sequential regenerative electro-Fenton. Environ. Sci. Technol. 49 (4), 2375–2383. https://doi.org/10.1021/es505679e.

Gao, X., Zhang, H., Wang, Y., Wang, H., Tang, Y., Hu, Y., Lv, Y., Bai, J., 2023. Study on preparation of a novel needle coke heterogeneous electro-Fenton cathode for coking wastewater treatment. Chem. Eng. J. 455, 140696. https://doi.org/10.1016/j.cej.2022.140696.

Ghasemi, M., Khataee, A., Gholami, P., Cheshmeh Soltani, R.D., 2019. Template-free microspheres decorated with Cu-Fe-NLDH for catalytic removal of gentamicin in heterogeneous electro-Fenton process. J. Environ. Manag. 248, 109236 https://doi.org/10.1016/j.jenvman.2019.07.007.

Gross, A.F., Sherman, E., Vajo, J.J., 2012. Aqueous room temperature synthesis of cobalt and zinc sodalite zeolitic imidizolate frameworks. Dalton Trans. 41 (18), 5458–5460. https://doi.org/10.1039/c2dt30174a.

Guo, M., Lu, M., Zhao, H., Lin, F., He, F., Zhang, J., Wang, S., Dong, P., Zhao, C., 2022. Efficient electro-Fenton catalysis by self-supported CFP@$CoFe_2O_4$ electrode. J. Hazard Mater. 423, 127033 https://doi.org/10.1016/j.jhazmat.2021.127033.

Harnisz, M., Korzeniewska, E., Gołaś, I., 2015. The impact of a freshwater fish farm on the community of tetracycline-resistant bacteria and the structure of tetracycline resistance genes in river water. Chemosphere 128, 134–141. https://doi.org/10.1016/j.chemosphere.2015.01.035.

Hu, J., Wang, S., Yu, J., Nie, W., Sun, J., Wang, S., 2021a. Duet Fe_3C and FeN_x sites for H_2O_2 generation and activation toward enhanced electro-Fenton performance in wastewater treatment. Environ. Sci. Technol. 55 (2), 1260–1269. https://doi.org/10.1021/acs.est.0c06825.

Hu, T., Deng, F., Feng, H., Zhang, J., Shao, B., Feng, C., Tang, W., Tang, L., 2021b. Fe/Co bimetallic nanoparticles embedded in MOF-derived nitrogen-doped porous carbon rods as efficient heterogeneous electro-Fenton catalysts for degradation of organic pollutants. Appl. Mater. Today 24, 101161. https://doi.org/10.1016/j.apmt.2021.101161.

Huang, X., Zhu, N., Mao, F., Ding, Y., Zhang, S., Liu, H., Li, F., Wu, P., Dang, Z., Ke, Y., 2020. Enhanced heterogeneous photo-Fenton catalytic degradation of tetracycline over yCeO_2/Fh composites: performance, degradation pathways, Fe^{2+} regeneration and mechanism. Chem. Eng. J. 392, 123636 https://doi.org/10.1016/j.cej.2019.123636.

Ishizaki, M., Tanno, H., Sutoh, H., Katsuki, T., Hayasaka, T., Yagi, M., Tsubonouchi, Y., Tajima, K., Kawamoto, T., Sakuda, Y., Kurihara, M., 2020. FeNi-layered double-hydroxide nanoflakes with potential for intrinsically high water-oxidation catalytic activity. ACS Appl. Energy Mater. 3 (9), 9040–9050. https://doi.org/10.1021/acsaem.0c01439.

Jia, X., Wang, Y., Tang, J., Song, K., Zhang, H., Lin, B., Zheng, H., 2023. FeNiLDH@Ni film modified stainless-steel as self-supported electrodes for efficient and stable overall water splitting in alkaline environments. Surf. Coating. Technol. 464, 129502 https://doi.org/10.1016/j.surfcoat.2023.129502.

Jiang, W., Cai, Y., Liu, D., Shi, Q., Wang, Q., 2023. Adsorption properties and mechanism of suaeda biochar and modified materials for tetracycline. Environ. Res. 235, 116549 https://doi.org/10.1016/j.envres.2023.116549.

Li, P., Zhao, R., Chen, H., Wang, H., Wei, P., Huang, H., Liu, Q., Li, T., Shi, X., Zhang, Y., Liu, M., Sun, X., 2019. Recent advances in the development of water oxidation electrocatalysts at mild pH. Small 15, 1805103. https://doi.org/10.1002/smll.201805103.

Li, X., Xiao, C., Ruan, X., Hu, Y., Zhang, C., Cheng, J., Chen, Y., 2021. Enrofloxacin degradation in a heterogeneous electro-Fenton system using a tri-metal-carbon nanofibers composite cathode. Chem. Eng. J. 427, 130927 https://doi.org/10.1016/j.cej.2021.130927.

Li, Y., Wang, C., Pan, S., Zhao, X., Liu, N., 2022. Mn doping improves in-situ H_2O_2 generation and activation in electro-Fenton process by Fe/Mn@CC cathode using high-temperature shock technique. Chemosphere 307, 136074. https://doi.org/10.1016/j.chemosphere.2022.136074.

Li, J., Zhong, D., Li, F., Li, K., Ma, W., Ma, J., Zhang, J., Sun, A., 2023. Efficient mineralization of coal pyrolysis wastewater in a heterogeneous electro-Fenton system using a novel Fe_3O_4-$LaFeO_3$/C/GF heterojunction cathode. Sep. Purif. Technol. 319, 124046 https://doi.org/10.1016/j.seppur.2023.124046.

Liu, X., Zhou, Y., Zhang, J., Luo, L., Yang, Y., Huang, H., Peng, H., Tang, L., Mu, Y., 2018. Insight into electro-Fenton and photo-Fenton for the degradation of antibiotics: mechanism study and research gaps. Chem. Eng. J. 347, 379–397. https://doi.org/10.1016/j.cej.2018.04.142.

Liu, L., Fang, L., Wu, F., Hu, J., Zhang, S., Luo, H., Hu, B., Zhou, M., 2020. Self-supported core-shell heterostructure MnO_2/NiCo-LDH composite for flexible high-performance supercapacitor. J. Alloys Compd. 824, 153929 https://doi.org/10.1016/j.jallcom.2020.153929.

Liu, D., Li, X., Ma, J., Li, M., Ren, F., Zhou, L., 2021a. Metal-organic framework modified pine needle-derived N, O-doped magnetic porous carbon embedded with Au nanoparticles for adsorption and catalytic degradation of tetracycline. J. Clean. Prod. 278, 123575 https://doi.org/10.1016/j.jclepro.2020.123575.

Liu, P., Zhong, D., Xu, Y., Zhong, N., He, G., 2021b. Co/Fe co-doped porous graphite carbon derived from metal organic framework for microelectrolysis-Fenton catalytic degradation of Rhodamine B. J. Environ. Chem. Eng. 9 (5), 105924 https://doi.org/10.1016/j.jece.2021.105924.

Liu, Y., Yang, Z., Wang, J., 2021c. Fenton-like degradation of sulfamethoxazole in Cu^0/Zn^0-air system over a broad pH range: performance, kinetics and mechanism. Chem. Eng. J. 403, 126320 https://doi.org/10.1016/j.cej.2020.126320.

Long, X., Shi, H., Huang, R., Gu, L., Liu, Y., He, C., Du, Y., Xiong, Z., Liu, W., Lai, B., 2023. Identifying the evolution of primary oxidation mechanisms and pollutant degradation routes in the electro-cocatalytic Fenton-like systems. J. Hazard Mater. 445, 130577 https://doi.org/10.1016/j.jhazmat.2022.130577.

Luo, T., Feng, H., Tang, L., Lu, Y., Tang, W., Chen, S., Yu, J., Xie, Q., Ouyang, X., Chen, Z., 2020. Efficient degradation of tetracycline by heterogeneous electro-Fenton process using Cu-doped Fe@Fe_2O_3: mechanism and degradation pathway. Chem. Eng. J. 382, 122970 https://doi.org/10.1016/j.cej.2019.122970.

Mahmoodi, N.M., Abdi, J., Taghizadeh, M., Taghizadeh, A., Hayati, B., Shekarchi, A.A., Vossoughi, M., 2019. Activated carbon/metal-organic framework nanocomposite: preparation and photocatalytic dye degradation mathematical modeling from wastewater by least squares support vector machine. J. Environ. Manag. 233, 660–672. https://doi.org/10.1016/j.jenvman.2018.12.026.

Oturan, M.A., Aaron, J.J., 2014. Advanced oxidation processes in water/wastewater treatment: principles and applications. A review. Crit. Rev. Environ. Sci. Technol. 44, 2577–2641. https://doi.org/10.1080/10643389.2013.829765.

Pacheco-Álvarez, M., Picos Benítez, R., Rodríguez-Narváez, O.M., Brillas, E., Peralta-Hernández, J.M., 2022. A critical review on paracetamol removal from different aqueous matrices by Fenton and Fenton-based processes, and their combined methods. Chemosphere 303, 134883. https://doi.org/10.1016/j.chemosphere.2022.134883.

Pan, Y., Zhang, Y., Zhou, M., Cai, J., Tian, Y., 2019. Enhanced removal of antibiotics from secondary wastewater effluents by novel UV/pre-magnetized Fe^0/H_2O_2 process. Water Res. 153, 144–159. https://doi.org/10.1016/j.watres.2018.12.063.

Peng, L., Yang, N., Yang, Y., Wang, Q., Xie, X., Sun-Waterhouse, D., Shang, L., Zhang, T., Waterhouse, G.I.N., 2021. Atomic cation-vacancy engineering of NiFe-layered double hydroxides for improved activity and stability towards the oxygen evolution reaction. Angew. Chem. Int. Ed. 60 (46), 24612–24619. https://doi.org/10.1002/anie.202109938.

Poudel, M.B., Kim, H.J., 2022. Confinement of Zn-Mg-Al-layered double hydroxide and α-Fe_2O_3 nanorods on hollow porous carbon nanofibers: a free-standing electrode for solid-state symmetric supercapacitors. Chem. Eng. J. 429, 132345 https://doi.org/10.1016/j.cej.2021.132345.

Qi, H., Sun, X., Sun, Z., 2022. Cu-doped Fe_2O_3 nanoparticles/etched graphite felt as bifunctional cathode for efficient degradation of sulfamethoxazole in the heterogeneous electro-Fenton process. Chem. Eng. J. 427, 131695 https://doi.org/10.1016/j.cej.2021.131695.

Qin, L., Sun, Q., Lai, C., Liu, S., Qin, X., Chen, W., Fu, Y., Zhou, X., Xu, F., Ma, D., 2023a. Sulfonic acid metal-organic frameworks derived iron-doped carbon as novel heterogeneous electro-Fenton catalysts for the degradation of tetracycline: performance and mechanism investigation. Chem. Eng. J. 474, 145722 https://doi.org/10.1016/j.cej.2023.145722.

Qin, X., Cao, P., Quan, X., Zhao, K., Chen, S., Yu, H., Su, Y., 2023b. Highly efficient hydroxyl radicals production boosted by the atomically dispersed Fe and Co sites for heterogeneous electro-Fenton oxidation. Environ. Sci. Technol. 57 (7), 2907–2917. https://doi.org/10.1021/acs.est.2c06981.

Ren, Y., Lin, L., Ma, J., Yang, J., Feng, J., Fan, Z., 2015. Sulfate radicals induced from peroxymonosulfate by magnetic ferrospinel MFe_2O_4 (M=Co, Cu, Mn, and Zn) as heterogeneous catalysts in the water. Appl. Catal. B Environ. 165, 572–578. https://doi.org/10.1016/j.apcatb.2014.10.051.

Shao, S., Hu, Y., Cheng, J., Chen, Y., 2019. Effects of carbon source, nitrogen source, and natural algal powder-derived carbon source on biodegradation of tetracycline (TEC). Bioresour. Technol. 288, 121567 https://doi.org/10.1016/j.biortech.2019.121567.

Sklari, S.D., Plakas, K.V., Petsi, P.N., Zaspalis, V.T., Karabelas, A.J., 2015. Toward the development of a novel electro-Fenton system for eliminating toxic organic substances from water. Part 2. Preparation, characterization, and evaluation of iron-impregnated carbon felts as cathodic electrodes. Ind. Eng. Chem. Res. 54 (7), 2059–2073. https://doi.org/10.1021/ie5048779.

Su, P., Zhang, J., Xiao, K., Zhao, S., Djellabi, R., Li, X., Yang, B., Zhao, X., 2020. C_3N_4 modified with single layer ZIF67 nanoparticles for efficient photocatalytic degradation of organic pollutants under visible light. Chin. J. Catal. 41 (12), 1894–1905. https://doi.org/10.1016/S1872-2067(20)63620-8.

Tian, Q., Xiao, F., Zhao, H., Fei, X., Shen, X., Postole, G., Zhao, G., 2020. Simultaneously accelerating the regeneration of Fe^{II} and the selectivity of 2e- oxygen reduction over sulfide iron-based carbon aerogel in electro-Fenton system. Appl. Catal. B Environ. 272, 119039 https://doi.org/10.1016/j.apcatb.2020.119039.

Wang, D., Zhao, F., Feng, J., Feng, H., Luo, J., Tang, W., 2022a. Ferrate modified carbon felt as excellent heterogeneous electro-Fenton cathode for chloramphenicol degradation. Water Res. 227, 119324 https://doi.org/10.1016/j.watres.2022.119324.

Wang, F.G., Liu, B., Wang, H.Y., Lin, Z.Y., Dong, Y.W., Yu, N., Luan, R.N., Chai, Y.M., Dong, B., 2022b. Motivating borate doped FeNi layered double hydroxides by molten salt method toward efficient oxygen evolution. J. Colloid Interface Sci. 610, 173–181. https://doi.org/10.1016/j.jcis.2021.12.031.

Wang, H., Tang, C., Wang, L., Sun, Z., Hu, X., 2023a. MOF-derived Co/Fe@NPC 500 with large amounts of low-valent metals as an electro-Fenton cathode for efficient degradation of ceftazidime. Appl. Catal. B Environ. 333, 122755 https://doi.org/10.1016/j.apcatb.2023.122755.

Wang, X., Zhang, Q., Jing, J., Song, G., Zhou, M., 2023b. Biomass derived S, N self-doped catalytic Janus cathode for flow-through metal-free electrochemical advanced oxidation process: better removal efficiency and lower energy consumption under neutral conditions. Chem. Eng. J. 466, 143283 https://doi.org/10.1016/j.cej.2023.143283.

Wu, Z., Gu, Y. ying, Xin, S., Lu, L., Huang, Z., Li, M., Cui, Y., Fu, R., Wang, S., 2022. Cu_xNi_yCo-LDH nanosheets on graphene oxide: an efficient and stable Fenton-like catalyst for dual-mechanism degradation of tetracycline. Chem. Eng. J. 434, 134574 https://doi.org/10.1016/j.cej.2022.134574.

Xia, Y., Yang, F., Zhang, B., Xu, C., Yang, W., Li, Y., 2021. Fabrication of novel FeS_2 NWs/Ti_3C_2 cathode for Photo-Electro-Fenton degradation of sulfamethazine. Chem. Eng. J. 426, 130719 https://doi.org/10.1016/j.cej.2021.130719.

Xin, S., Huo, S., Xin, Y., Gao, M., Wang, Y., Liu, W., Zhang, C., Ma, X., 2022. Heterogeneous photo-electro-Fenton degradation of tetracycline through nitrogen/oxygen self-doped porous biochar supported $CuFeO_2$ multifunctional cathode catalyst under visible light. Appl. Catal. B Environ. 312, 121442 https://doi.org/10.1016/j.apcatb.2022.121442.

Xiong, J., Zeng, H., Peng, J., Wang, L., Peng, D., Liu, F., Xu, S., Yang, Z., 2023. Fabrication of Cu_2O/ZnTi-LDH p-n heterostructure by grafting Cu_2O NPs onto the LDH host layers from Cu-doped ZnTi-LDH and insight into the photocatalytic mechanism. Compos. Part B-Eng. 250, 110447 https://doi.org/10.1016/j.compositesb.2022.110447.

Xu, L., Ouyang, W., Qian, Y., Su, C., Su, J., Chen, H., 2016. High-throughput profiling of antibiotic resistance genes in drinking water treatment plants and distribution systems. Environ. Pollut. 213, 119–126. https://doi.org/10.1016/j.envpol.2016.02.013.

Xu, M., Wei, J., Cui, X., Li, J., Pan, G., Li, Y., Jiang, Z., Niu, X., Cui, N., Li, J., 2023. High-efficiency electro-Fenton process based on in-situ grown CoFeCe-LDH@CFs free-standing cathodes: correlation of cerium and oxygen vacancies with H_2O_2. Chem. Eng. J. 455, 140922 https://doi.org/10.1016/j.cej.2022.140922.

Yan, J., Peng, J., Lai, L., Ji, F., Zhang, Y., Lai, B., Chen, Q., Yao, G., Chen, X., Song, L., 2018. Activation $CuFe_2O_4$ by hydroxylamine for oxidation of antibiotic sulfamethoxazole. Environ. Sci. Technol. 52 (24), 14302–14310. https://doi.org/10.1021/acs.est.8b03340.

Yan, L., Du, Z., Lai, X., Lan, J., Liu, X., Liao, J., Feng, Y., Li, H., 2023. Synergistically modulating the electronic structure of Cr-doped FeNi LDH nanoarrays by O-vacancy and coupling of MXene for enhanced oxygen evolution reaction. Int. J. Hydrogen Energy 48 (5), 1892–1903. https://doi.org/10.1016/j.ijhydene.2022.10.087.

Ye, Z., Zhang, W., Lanzalaco, S., Zhao, L., Sirés, I., Xia, P., Zhai, J., He, Q., 2023. Ultra-uniform MIL-88B(Fe)/Fe_3S_4 hybrids engineered by partial sulfidation to boost catalysis in electro-Fenton treatment of micropollutants: experimental and mechanistic insights. Chem. Eng. J. 455, 140757 https://doi.org/10.1016/j.cej.2022.140757.

Zhang, W., Zhang, H., Yan, X., Zhang, M., Luo, R., Qi, J., Sun, X., Shen, J., Han, W., Wang, L., Li, J., 2020. Controlled synthesis of bimetallic Prussian blue analogues to activate peroxymonosulfate for efficient bisphenol A degradation. J. Hazard Mater. 387, 121701 https://doi.org/10.1016/j.jhazmat.2019.121701.

Zhang, Y., Wang, P., Yang, J., Lu, S., Li, K., Liu, G., Duan, Y., Qiu, J., 2021. Decorating ZIF-67-derived cobalt–nitrogen doped carbon nanocapsules on 3D carbon frameworks for efficient oxygen reduction and oxygen evolution. Carbon 177, 344–356. https://doi.org/10.1016/j.carbon.2021.02.052.

Zhang, J., Qiu, S., Feng, H., Hu, T., Wu, Y., Luo, Ting, Tang, W., Wang, D., 2022a. Efficient degradation of tetracycline using core–shell Fe@Fe_2O_3-CeO_2 composite as novel heterogeneous electro-Fenton catalyst. Chem. Eng. J. 428, 131403 https://doi.org/10.1016/j.cej.2021.131403.

Zhang, J., Wang, D., Zhao, F., Feng, J., Feng, H., Luo, J., Tang, W., 2022b. Ferrate modified carbon felt as excellent heterogeneous electro-Fenton cathode for chloramphenicol degradation. Water Res. 227, 119324 https://doi.org/10.1016/j.watres.2022.119324.

Zhao, H., Wang, Y., Wang, Y., Cao, T., Zhao, G., 2012. Electro-Fenton oxidation of pesticides with a novel Fe_3O_4@Fe_2O_3/activated carbon aerogel cathode: high activity, wide pH range and catalytic mechanism. Appl. Catal. B Environ. 125, 120–127. https://doi.org/10.1016/j.apcatb.2012.05.044.

Zhao, H., Ma, X., Lu, M., He, F., Lin, F., Zhang, Y., Zhang, J., Dong, P., Zhao, C., Sun, H., 2023. Melamine foam derived nitrogen and boron co-doped metal-free electrode for enhanced electro-Fenton degradation of metronidazole. Chem. Eng. J. 455, 140593 https://doi.org/10.1016/j.cej.2022.140593.

Zheng, X., Chu, Y., Miao, B., Fan, J., 2022. Ag-doped Bi_2WO_6/BiOI heterojunction used as photocatalyst for the enhanced degradation of tetracycline under visible-light and biodegradability improvement. J. Alloys Compd. 893, 162382 https://doi.org/10.1016/j.jallcom.2021.162382.

Zhong, W., Gong, Z., He, Z., Zhang, N., Kang, X., Mao, X., Chen, Y., 2023. Modulating surface oxygen species via facet engineering for efficient conversion of nitrate to ammonia. J. Energy Chem. 78, 211–221. https://doi.org/10.1016/j.jechem.2022.11.024.

Zhou, J., Ma, F., Guo, H., Su, D., 2020. Activate hydrogen peroxide for efficient tetracycline degradation via a facile assembled carbon-based composite: synergism of powdered activated carbon and ferroferric oxide nanocatalyst. Appl. Catal. B Environ. 269, 118784 https://doi.org/10.1016/j.apcatb.2020.118784.

Zhou, Q., Hong, P., Shi, X., Li, Y., Yao, K., Zhang, W., Wang, C., He, J., Zhang, K., Kong, L., 2023. Efficient degradation of tetracycline by a novel nanoconfinement structure Cu_2O/Cu@MXene composite. J. Hazard Mater. 448, 130995 https://doi.org/10.1016/j.jhazmat.2023.130995.

Zhu, Y., Qiu, S., Deng, F., Zheng, Y., Li, K., Ma, F., Liang, D., 2019. Enhanced degradation of sulfathiazole by electro-Fenton process using a novel carbon nitride modified electrode. Carbon 145, 321–332. https://doi.org/10.1016/j.carbon.2019.01.032.

Zhu, D., Zhen, Q., Xin, J., Ma, H., Pang, H., Tan, L., Wang, X., 2021. In situ hierarchical encapsulation of bimetallic selenides into honeycomb-like nitrogen doped porous carbon nanosheets for highly sensitive and selective guanosine detection. J. Colloid Interface Sci. 598, 181–192. https://doi.org/10.1016/j.jcis.2021.04.048.

Zou, R., Chen, Z., Zhong, L., Yang, W., Li, T., Gan, J., Yang, Y., Chen, Z., Lai, H., Li, X., Liu, C., Admassie, S., Iwuoha, E., Lu, J., Peng, X., 2023. Nanocellulose-assisted molecularly engineering of nitrogen deficient graphitic carbon nitride for selective biomass photo-oxidation. Adv. Funct. Mater. 33, 2301311 https://doi.org/10.1002/adfm.202301311.